SOLITONS

PACS numbers: 42.65.Tg; 42.82.Et
DOI: 10.1070/QE2003v033n11ABEH002539

Dark spatial optical solitons in planar gradient waveguides in the *Z*-cut of the 3*m* symmetry crystals

M.N. Frolova, M.V. Borodin, S.M. Shandarov, V.M. Shandarov, Yu.M. Larionov

***Abstract*. The propagation of light beams is studied in a planar photorefractive waveguide fabricated by high-temperature diffusion of metal ions in the *Z*-cut substrate of the 3*m* symmetry crystal. The wave equations are obtained for single-mode light beams with TE and TM polarisations in planar diffusion waveguides, which take into account the two-dimensional distribution of the optical field. Expressions are found for a nonlinear change in the refractive index when the photovoltaic mechanism makes a dominant contribution to the photorefractive effect. The propagation of single-mode light beams is analysed numerically for a Ti : Fe : $LiNbO_3$ waveguide fabricated by the successive diffusion of titanium and iron into lithium niobate. It is shown that single-mode light beams with a smooth amplitude envelope can propagate without significant changes in the region of a dip in the intensity modelling a dark soliton. The relations between the amplitude and width of a dark spatial soliton are obtained for the TM modes of a photorefractive planar waveguide.**

Keywords: *photorefractive crystals, planar waveguides, spatial solitons.*

1. Introduction

The self-action of light beams in photorefractive crystals is observed at low intensities and provides the propagation of the beams preserving the envelope in the form of bright and dark solitons [1 – 5]. Similar effects can also take place in planar waveguides fabricated on photorefractive crystal substrates [6 – 9]. In this case, the formation of spatial solitons can be optimised by controlling the photorefractive parameters of a medium during the fabrication of a waveguide layer by diffusion or epitaxial methods, as well as by ion implantation.

Lithium niobate ($LiNbO_3$) and lithium tantalate ($LiTaO_3$) crystals, belonging to the trigonal class of the 3*m* symmetry, are attractive for producing waveguide spatial solitons. The methods for fabricating waveguide layers in these crystals are well developed [10, 11], and doping with impurities of Fe, Cu, Mg, etc. allows one to vary the photorefractive properties of the substrate and waveguide in a broad range [12, 13]. The formation of dark spatial solitons in such waveguides opens up the possibility of inducing channel waveguides for radiation at other wavelengths, i.e., provides the optical control of light beams.

M.N. Frolova, M.V. Borodin, S.M. Shandarov, V.M. Shandarov, Yu.M. Larionov Tomsk State University of Control Systems and Radioelectronics, prosp. Lenina 40, 634050 Tomsk, Russia; e-mail: frolova@phys.tsu.ru

Received 12 November 2002; revision received 19 March 2003
Kvantovaya Elektronika **33** (11) 1001 – 1006 (2003)
Translated by M.N. Sapozhnikov

2. Wave equations for the TE and TM light beams in planar diffusion waveguides

Consider a planar waveguide prepared on a plate made of a uniaxial electrooptical crystal (Fig. 1). We assume that the optic axis Z of the crystal is directed along the normal to the waveguide layer-cover medium (air) interface with the refractive index $N_c = 1$. The ordinary and extraordinary refractive indices of the waveguide structure can be written in the form

$$N_o(x, y, z) = N_{os} + \Delta N_{ow}(z) + \delta N_o(x, y, z), \quad (1)$$

$$N_e(x, y, z) = N_{es} + \Delta N_{ew}(z) + \delta N_e(x, y, z), \quad (2)$$

where N_{os} and N_{es} are the ordinary and extraordinary refractive indices of the substrate; ΔN_{ow} and ΔN_{ew} are the additions, which are decreasing functions for $z < 0$ and are caused by the inhomogeneous distribution of the impurity; and δN_o and δN_e are the nonlinear additions to the refractive indices caused by self-action effects. In the case of a diffusion waveguide and the photorefractive mechanism of optical nonlinearity, the additions to the refractive indices satisfy the inequalities

$$\Delta N_{ow} \ll N_{os}, \ \Delta N_{ew} \ll N_{es}, \quad (3)$$

$$\delta N_o \ll \Delta N_{ow}, \ \ \delta N_e \ll \Delta N_{ew}. \quad (4)$$

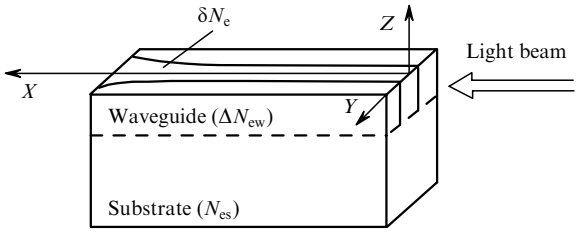

Figure 1. Propagation geometry of a light beam in a nonlinear planar waveguide.

Inequalities (3) and (4) suggest that light waves, directed due to waveguide properties and optical nonlinearity, can propagate at small angles to the longitudinal axis of the waveguide (the x axis). In this case, if the nondiagonal components of the permittivity tensor are not perturbed in the waveguide, we can consider the propagation of the TE and TM waves. The corresponding wave equations, describing the propagation of light beams along the x axis, for the dominating components of the electric field vector of the light field E_y (the TE wave) and E_z (the TM wave) can be obtained from Maxwell's equations in the form

$$\frac{\partial^2 E_y}{\partial x^2}+\frac{\partial^2 E_y}{\partial y^2}+\frac{\partial^2 E_y}{\partial z^2}+k_0^2 N_o^2 E_y=0, \tag{5}$$

$$\frac{\partial^2 E_z}{\partial x^2}+\frac{\partial^2 E_z}{\partial y^2}+\frac{N_e^2}{N_o^2}\frac{\partial^2 E_z}{\partial z^2}+k_0^2 N_e^2 E_z=0, \tag{6}$$

where $k_0=2\pi/\lambda$ is the wave number in vacuum. Under the assumptions made above, equation (5) for the TE waves is exact. We have derived equation (6) for the TE waves by neglecting a weak dependence of the ratio N_e^2/N_o^2 on the coordinate z.

The distributions of the TE and TM fields in selectively excited single-mode beams can be represented in the same form

$$E_y^{\mathrm{TE}}(x,y,z)=\Psi_y(z)A^{\mathrm{TE}}(x,y)\exp\left(-\mathrm{i}\beta^{\mathrm{TE}}x\right), \tag{7}$$

$$E_z^{\mathrm{TM}}(x,y,z)=\Psi_z(z)A^{\mathrm{TM}}(x,y)\exp\left(-\mathrm{i}\beta^{\mathrm{TM}}x\right), \tag{8}$$

where $\Psi_y(z)$ and $\Psi_z(z)$ determine the transverse distributions of fields in the TE and TM modes of a planar waveguide with the propagation constants β^{TE} and β^{TM}, and the amplitudes $A^{\mathrm{TE,TM}}(x,y)$ of the beams are assumed slowly varying functions of the longitudinal coordinate x. In this case, the transverse distribution of the field of the TE_m mode with the number $m=0, 1, 2, \ldots$ in a planar waveguide satisfies the equation [14]

$$\frac{\mathrm{d}^2\Psi_y^{(m)}}{\mathrm{d}z^2}+k_0^2\left[(N_{\mathrm{os}}+\Delta N_{\mathrm{ow}}(z))^2-(N_m^*)^2\right]\Psi_y^{(m)}=0, \tag{9}$$

where $N_m^*=\beta_m^{\mathrm{TE}}/k_0$ is the effective refractive index of the mode. By substituting the field distribution (7) for a single-mode TE beam into equation (5), we obtain the truncated wave equation for the evolution of the beam amplitude $A_m^{\mathrm{TM}}(x,y)$ taking into account its slow variation along the x axis, inequalities (3) and (4), equation (9), and the orthogonality of the modes:

$$\left(\frac{\partial}{\partial x}+\frac{\mathrm{i}}{2k_0N_m^*}\frac{\partial^2}{\partial y^2}\right)A_m^{\mathrm{TE}}(x,y)$$

$$=-\mathrm{i}k_0\delta\tilde{N}_{om}(x,y)A_m^{\mathrm{TE}}(x,y). \tag{10}$$

We have derived equation (10) assuming that $N_m^*\simeq N_{\mathrm{os}}$ and introducing the nonlinear addition to the refractive index of the mth mode averaged over the coordinate z:

$$\delta\tilde{N}_{om}(x,y)=\frac{\int_{-\infty}^{\infty}\Psi_y^{(m)}(z)\delta N_{\mathrm{o}}(x,y,z)\Psi_y^{(m)}(z)\mathrm{d}z}{\int_{-\infty}^{\infty}\left[\Psi_y^{(m)}(z)\right]^2\mathrm{d}z}. \tag{11}$$

The use of the approximate relation $N_e^2/N_o^2\simeq N_{\mathrm{es}}^2/N_{\mathrm{os}}^2$ in the analysis of the TM_p modes of an anisotropic planar waveguide allows us to write the corresponding wave equation for the transverse distribution of the field in the form [15]

$$\frac{\mathrm{d}^2\Psi_z^{(p)}}{\mathrm{d}z^2}+k_0^2\frac{N_{\mathrm{os}}^2}{N_{\mathrm{es}}^2}\left[(N_{\mathrm{es}}+\Delta N_{\mathrm{ew}}(z))^2-(N_p^*)^2\right]\Psi_z^{(p)}=0, \tag{12}$$

where $N_p^*=\beta_p^{\mathrm{TM}}/k_0$. The evolution of the amplitude $A_p^{\mathrm{TM}}(x,y)$ of a single-mode beam can be described in this case by the equation

$$\left(\frac{\partial}{\partial x}+\frac{\mathrm{i}}{2k_0N_p^*}\frac{\partial^2}{\partial y^2}\right)A_p^{\mathrm{TM}}(x,y)$$

$$=-\mathrm{i}k_0\delta\tilde{N}_{ep}(x,y)A_p^{\mathrm{TM}}(x,y) \tag{13}$$

with the averaged nonlinear addition

$$\delta\tilde{N}_{ep}(x,y)=\frac{\int_{-\infty}^{\infty}\Psi_z^{(p)}(z)\delta N_{\mathrm{e}}(x,y,z)\Psi_z^{(p)}(z)\mathrm{d}z}{\int_{-\infty}^{\infty}\left[\Psi_z^{(p)}(z)\right]^2\mathrm{d}z}. \tag{14}$$

3. Nonlinear additions to the refractive index in photorefractive planar waveguides

Photoinduced variations in the properties of a photorefractive waveguide are caused by photoexcitation of charge carriers and their redistribution over impurity centres. A complicated three-dimensional distribution of the electric field $\boldsymbol{E}^{\mathrm{sc}}(x,y,z)$ formed in the waveguide leads to perturbations of the refractive index of the waveguide due to a linear electrooptical effect. Under stationary conditions of continuous irradiation in the absence of trap saturation, the density distribution of photoexcited and thermally generated charge carriers can be represented in the form

$$n(x,y,z)=n_{\mathrm{d}}(z)+G(z)|\boldsymbol{E}(x,y,z)|^2. \tag{15}$$

Here, $n_{\mathrm{d}}(z)$ and $G(z)$ are the dark concentration of free charge carriers and the photogeneration parameter, respectively, which depends on the coordinate z because of the inhomogeneous distribution of impurity centres in the waveguide.

The redistribution of charges in the crystal in the absence of an external field occurs due to diffusion, photovoltaic effect, and drift of the spatial charge $\boldsymbol{E}^{\mathrm{sc}}$ in the internal field formed in the crystal. In lithium niobate and tantalate crystals doped with Fe and Cu, the photorefractive effect is predominantly determined by the photovoltaic mechanism [16]. In this case, the diffusion current can be neglected, and the stationary distribution of the spatial-charge field can be found from the continuity equation

$$\mathrm{div}\left(\boldsymbol{\delta}^{\mathrm{c}}+\boldsymbol{\delta}^{\mathrm{ph}}\right)=0, \tag{16}$$

where $\boldsymbol{\delta}^{\mathrm{c}}$ and $\boldsymbol{\delta}^{\mathrm{ph}}$ are the density vectors of conduction and photovoltaic currents with components $\delta_m^{\mathrm{c}}=en\mu_{mn}E_n^{\mathrm{sc}}$ and $\delta_m^{\mathrm{ph}}=\beta_{mij}E_iE_j^*$, respectively; μ_{mn} and β_{mij} are the components of the mobility tensor of charge carriers and the photovoltaic tensor, respectively; E_n^{sc} are the components of the electric strength of the spatial charge field; and e is the elementary electric charge.

We will also take into account that photoconductivity and photovoltaic current are mainly determined by the dominating components of the light field (E_y and E_z for the TE and TM waves, respectively) and take into consideration the symmetry of the photovoltaic tensor and relations between its experimentally measured components ($\beta_{22} \ll \beta_{33}$, β_{31}, where matrix notation is used below) for $Fe : LiNbO_3$, $Fe : LiTaO_3$, and $Cu : LiNbO_3$ crystals [16]. In addition, according to inequalities (4), the characteristic size of the spatial inhomogeneity of the light field along the z axis is substantially smaller that that along the y axis. This suggests that the charge separation in the waveguide mainly occurs along the z axis, and equation (16) can be simplified. For a crystal opened along this axis, this equation will have the following approximate solutions

$$E_{sc}^{TE}(x,y,z) = -\frac{\beta_{31}(z)\Psi_y^2(z)\left|A^{TE}(x,y)\right|^2}{\sigma_d(z) + B_{ph}(z)\Psi_y^2(z)\left|A^{TE}(x,y)\right|^2}, \quad (17)$$

$$E_{sc}^{TM}(x,y,z) = -\frac{\beta_{33}(z)\Psi_z^2(z)\left|A^{TM}(x,y)\right|^2}{\sigma_d(z) + B_{ph}(z)\Psi_z^2(z)\left|A^{TM}(x,y)\right|^2}, \quad (18)$$

where $E_{sc}^{TE,TM}$ is the z component of the spatial charge field strength, induced by the TE and TM waves; $\sigma_d = e\mu_3 n_d$ is the dark conductivity; $B_{ph} = e\mu_3 G$ is the photoconductivity coefficient; μ_3 is the tensor component corresponding to the mobility of charge carriers along the z axis. Relations (17) and (18) were derived taking into account the dependence of the components β_{31} and β_{33} of the photovoltaic tensor on the transverse coordinate z, which is caused by the inhomogeneous distribution of impurities, and relations (7), (8), and (15) were used.

Taking into account the form of the electrooptical tensor for the symmetry $3m$ crystals, we obtain the nonlinear additions to the refractive index:

$$\delta N_o(x,y,z) = -\frac{1}{2} N_{os}^3 r_{13} E_{sc}^{TE}(x,y,z) \quad (19)$$

for the TE light beam and

$$\delta N_e(x,y,z) = -\frac{1}{2} N_{es}^3 r_{33} E_{sc}^{TM}(x,y,z) \quad (20)$$

for the TM light beam.

Therefore, the self-action of light beams propagating in diffusion photorefractive waveguides on the Z-cut of $LiNbO_3$ and $LiTaO_3$ crystals is described by relations (9)–(11), (17), (19) for the TE waves and (12)–(14), (18), (20) for the TM waves.

4. Parameters of a model waveguide

We analysed numerically the propagation of light beams in a model waveguide produced by a successive high-temperature diffusion of Ti and Fe into a lithium niobate plate oriented along the Z axis. This waveguide maintained six TM modes at a wavelength of 633 nm, and its refractive-index profile at the depth $0 \geqslant z > -9$ μm was well approximated by the function

$$N_e(z) = N_{es} + \frac{\Delta N_e}{\cosh^2(z/h_w)} \quad (21)$$

with the parameters $\Delta N_e = 0.0101$, $h_w = 8.5$ μm, and $N_{es} = 2.200$. The dependence $N_e(z)$ is shown in Fig. 2 by a solid curve together with the values of the effective refractive index n_p^* obtained experimentally and calculated from the known dispersion equation. The wave equation (12) for the refractive index profile described by function (21) has analytic solutions [17]. Figure 3 shows the distributions of the fields $\Psi^{(p)}(z)$ for the $TM_0 - TM_3$ modes of a planar waveguide under study normalised according to the condition $h_w^{-1}\int_{-\infty}^{\infty}[\Psi^{(p)}(z)]^2 dz = 1$. The experimental study of nonlinear intermode interference in this waveguide [18] showed that the relaxation time of induced variations in the refractive index of the waveguide increases with the waveguide-mode number and lies in the range between 1 and 20 s. The magnitude of the induced variations increases with the light intensity and mode number. These features are typical for waveguides whose photorefractive properties and conductivity are determined by the inhomogeneous distribution of Fe^{2+} and Fe^{3+} ions in the waveguide layer [19].

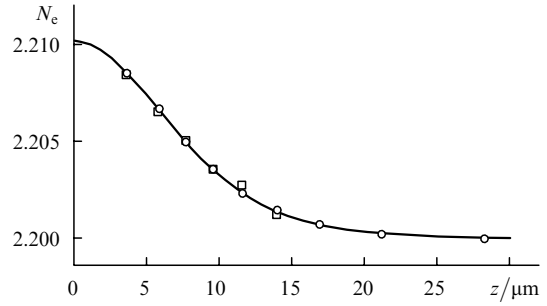

Figure 2. Profile of the refractive index of a planar $Ti : Fe : LiNbO_3$ waveguide (solid curve) and the calculated (circles) and experimental (squares) values of the effective refractive index.

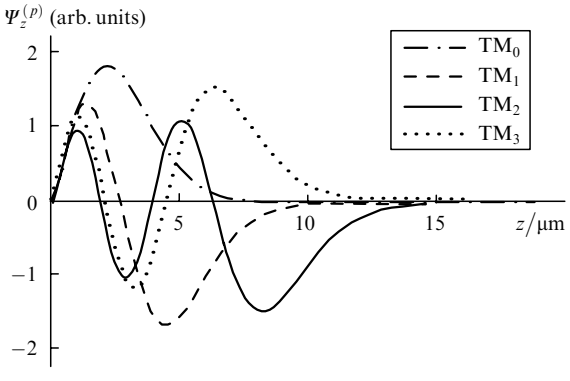

Figure 3. Normalised transverse light-field distributions for the $TM_0 - TM_3$ modes in a $Ti : Fe : LiNbO_3$ planar waveguide.

When the mass concentration of iron ions exceeds, as in our case, 1 % near the waveguide layer–cover medium interface (for $z = 0$, Fig.1), the dark conductivity is substantially higher than photoconductivity [20] ($\sigma_d(z) \gg B_{ph}(z)\Psi_z^2(z)|A(x,y)|^2$) for the $TM_0 - TM_3$ waveguide modes. Both the dark conductivity $\sigma_d(z)$ and the photovoltaic constant $\beta_{33}(z)$ decrease with distance from the boundary $z = 0$ with decreasing the concentration of iron ions. However, an increase in the photorefractive response

with the mode number suggests that $\sigma_d(z)$ decreases faster than $\beta_{33}(z)$. We neglected the photoconductivity in numerical calculations, and described the dependences of these quantities on z by the functions

$$\beta_{33}(z) = \beta_0 \exp\left(\frac{z}{h_{ph}}\right) + \beta_s, \tag{22}$$

and

$$\sigma_d(z) = \sigma_0 \exp\left(\frac{z}{h_d}\right) + \sigma_s \tag{23}$$

with the parameters $\beta_0 = -1 \times 10^{-10}$ A W^{-1}, $\beta_s = -10^{-12}$ A W^{-1}, $\sigma_0 = 7 \times 10^{-10}$ Ω^{-1} m^{-1}, $\sigma_s = 10^{-15}$ Ω^{-1} m^{-1}, $h_{ph} = 10$ μm, and $h_d = 2$ μm. The choice of a negative sign of the photovoltaic coefficient for the positive electrooptical constant $r_{33} = 30.8$ pm V^{-1} [21] provides the defocusing nonlinearity, which is typical of Fe : $LiNbO_3$ crystals.

Note that the refractive index profile described by expression (21) can be used for the description of lithium niobate waveguides produced by the high-temperature diffusion of metal ions by varying technological parameters in a rather broad range. The approximation of the dependence $\beta_{33}(z)$ by exponential function (22) is justified for structures into which a photosensitive impurity (Fe, Cu,, etc.) is doped by diffusion, following the formation of a waveguide layer, from sufficiently thick films. In the case of diffusion from thin films and long annealing times, the distribution of the impurity photosensitivity in the waveguide and, hence, the dependence $\beta_{33}(z)$ can be described by a Gaussian or the error function [11]. If the Cu ions are used as a photosensitive impurity, then, along with the dark conductivity of the waveguide, the photoconductivity should be also taken into account upon formation of the waveguide in weakly doped Fe : $LiNbO_3$ crystals.

5. Dark spatial solitons in bulk crystals and planar waveguides

In homogeneous bulk media of the type Fe : $LiNbO_3$ with the dominating dark conductivity, dark spatial photovoltaic solitons of the Kerr type can propagate with the envelope [5]

$$A(x,z) = A(0,z) = A_0 \tanh\left(\frac{z}{b}\right), \tag{24}$$

where the amplitude A_0 and width b of a dark soliton are related by the expression

$$b = \frac{\sqrt{2}}{A_0 k_0 N_{es}^2 \left(r_{33}\beta_{33}\sigma_d^{-1}\right)^{1/2}}. \tag{25}$$

The amplitude A_0 in real experiments is a smooth function of the transverse coordinates b and y, and relation (25) can be used to estimate A_0 at the beam centre at $y = z = 0$.

The inhomogeneity of the field over the coordinate z in this waveguide structure is uniquely determined by the mode distribution $\Psi_z^{(p)}(z)$, and the soliton envelope can be defined as the function $A(x,y)$ of the transverse coordinate y. Indeed, in the case of a negligible photoconductivity and TM waves, it follows from equations (14), (18), and (20) that the nonlinear addition to the refractive index has a simple form

$$\delta N_{ep}(x,y) = \frac{1}{2} N_{es}^3 r_{33} \tilde{f} \left|A^{TM}(x,y)\right|^2, \tag{26}$$

where the parameter $\tilde{f}$ takes into account the inhomogeneity of the distributions of the photovoltaic current, dark conductivity, and the waveguide-mode field over the coordinate z:

$$\tilde{f} = \frac{\int_{-\infty}^{\infty} [\beta_{33}(z)/\sigma_d(z)] \left[\Psi_z^{(p)}(z)\right]^4 dz}{\int_{-\infty}^{\infty} \left[\Psi_z^{(p)}(z)\right]^2 dz}. \tag{27}$$

In this case, equation (13) has a solution in the form of a dark Kerr soliton,

$$A(x,y) = A(0,y) = A_0 \tanh\left(\frac{y}{b}\right) \tag{28}$$

with a dip of width b in the intensity distribution along the transverse coordinate y and the amplitude

$$A_0 = \frac{\sqrt{2}}{b k_0 N_{es}^2 \left(r_{33}\tilde{f}\right)^{1/2}}. \tag{29}$$

The waveguide parameter $\tilde{f}$ increases with the waveguide mode number, and is equal to 2.58×10^{-3}, 3.99×10^{-3}, 6.53×10^{-3}, and 1.10×10^{-2} m V^{-1} for the TM_0, TM_1, TM_2, and TM_3 modes, respectively. Therefore, the maximum value of the light-field amplitude A_0 required to obtain a dark spatial soliton corresponds to the TM_0 mode. In the case of this mode, for the width of the dip $b = 10$ μm and the wavelength 633 nm, it is necessary to excite a beam with the amplitude $A_0 = 1.045 \times 10^4$ V m^{-1} in the waveguide to produce a dark soliton.

6. Analysis of the influence of the beam envelope on the propagation of dark spatial solitons

Because in real experiments the beams with envelopes of a finite width are used, we simulated numerically the propagation of light beams for different waveguide modes at the input amplitude distributions corresponding to a dark Kerr soliton overlapped on the envelopes of three types:

$$A^{TM}(0,y) = A_0 \exp\left(-\frac{y^2}{2a^2}\right) \tanh\left(\frac{y}{b}\right), \tag{30}$$

$$A^{TM}(0,y) = A_0 \exp\left(-\frac{y^6}{2a^6}\right) \tanh\left(\frac{y}{b}\right), \tag{31}$$

$$A^{TM}(0,y) = A_0 \left[\tanh\left(\frac{a-y}{a_0}\right) + \tan\left(\frac{a+y}{a_0}\right)\right] \tanh\left(\frac{y}{b}\right). \tag{32}$$

The evolution of the spatial distribution of the beam amplitude with the dip width $b = 10$ μm and the characteristic size of the smooth envelope $a = 120$ μm is illustrated in Fig. 4. The beam amplitude $A_0 = 1.1 \times 10^4$ V m^{-1} was chosen greater than the value $A_{00} = 1.045 \times 10^4$ V m^{-1} required to obtain a perfect dark soliton of type (28) at the TM_0 mode of the planar waveguide under study. In this case, the distribution of the beam amplitude in the region of the dip upon propagation over the distance $l = 15$ mm

changes rather weakly. The maximum variations in this region are observed for the most smooth envelope described by a Gaussian. However, the envelope itself in this region changes much stronger in the case of the six-order super-Gaussian distribution (31) and 'rectangular' function (32). Figure 4a shows distortions in the beam shape for the Gaussian envelope in the absence of nonlinearity, when the uncompensated diffraction divergence causes a significant distortion of the envelope and spreading of a dark dip.

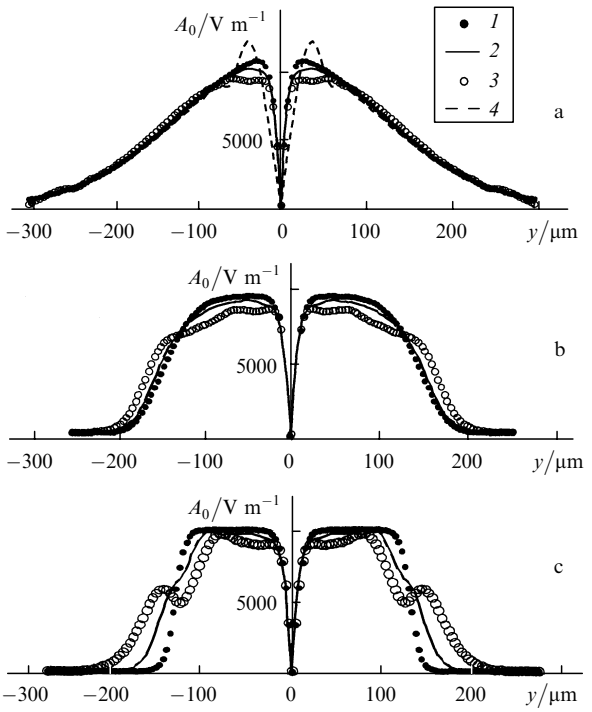

Figure 4. Light-field distributions at the waveguide input (*1*) and after the propagation of a beam by 7.5 (*2*) and 15 mm (*3*) for the Gaussian (a), six-order super-Gaussian (b) and 'rectangular' (c) envelopes for the width of a dip in the intensity modelling a dark soliton $b = 10$ μm; curve (*4*) is the distribution of the beam amplitude propagated by 15 mm in the absence of nonlinearity (a).

The increase of the dip b width up to 20 μm with the proportional decrease in the amplitude A_0 down to 5.5×10^3 V m^{-1} does not change significantly the distribution at the central part of the dip but reduces distortions of its shape during the beam propagation due to a decrease in optical nonlinearity ($\delta N_e \sim A_0^2$). However, when the beam width decreases down to $a = 80$ μm, the dip in the output distribution $A(l, y)$ increases noticeably and the regime of propagation of a dark spatial soliton is violated strictly speaking. Figure 5 shows the input and output distributions of the light field for a beam with Gaussian envelopes with $a = 80$ and 150 μm. Note that the difference between the distributions $A(0, y)$ and $A(l, y)$ is comparatively small even for $a = 80$ μm, and can be unnoticed in the experimental realisation of a dark soliton.

Figure 6 shows the pictures of propagation of the TM_0 beam with the input distribution $A^{TM}(0, y)$ described by expression (31) with different amplitudes. When the amplitude was reduced below its optimal value ($A_{00} = 5.5 \times 10^3$ V m^{-1}), the dip width being fixed, focusing became insufficient (Fig. 6b) and the regime of propagation of a dark

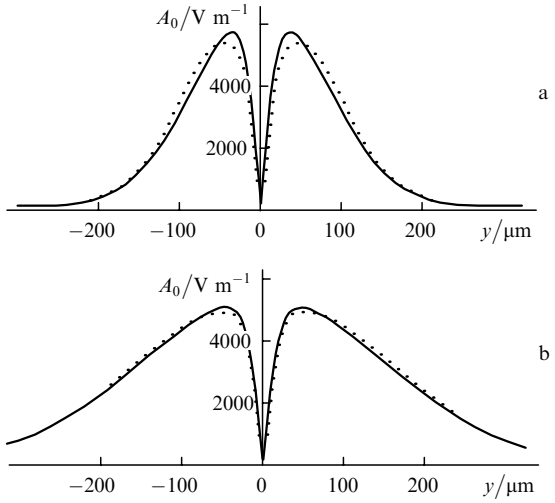

Figure 5. Light-field distributions at the crystal input (solid curves) and after the propagation of a beam by 15 mm (point curves) for the Gaussian envelope with the half-width a =80 (a) and 150 μm (b).

spatial soliton was violated. Too sharp focusing observed when the amplitude exceeded A_{00} (Fig. 6c), although violates the regime of propagation of a perfect soliton, almost does not change the width of the dark dip overt the crystal length of 30 mm. Note that a decrease in the refractive index induced by light beams with the amplitude distributions under study for $|y| > b$ can be used to realise the waveguide propagation of light from another spectral region, where the photorefractive properties of a medium are not observed [6, 7]. The results presented in Figs 4–6 illustrate the possibility of fabricating channel waveguides of this type in Ti : Fe : $LiNbO_3$ planar structures. The light-field amplitudes $A_0 \sim 10^4$ V m^{-1} required for producing dark spatial

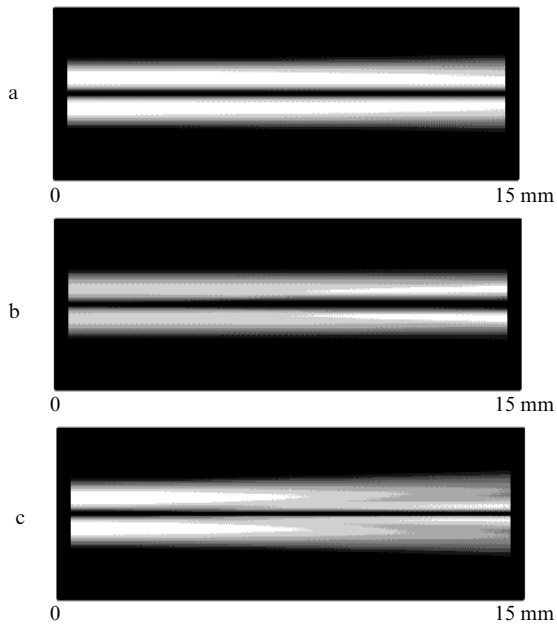

Figure 6. Intensity distributions for a light beam with the super-Gaussian envelope along the x axis in a 15-mm thick crystal for $A_0 = 5.6 \times 10^3$ (a), 1.9×10^3 (b), and 9.3×10^3 V m^{-1} (c). The vertical scale is magnified by a factor of 14.

solitons with the envelopes considered above are provided in the waveguide under study at the input radiation power ~ 1 mW.

7. Conclusions

We have analysed the propagation of single-mode light beams selectively excited in photorefractive gradient planar waveguides with the help of the wave equation derived in the paper in the paraxial approximation with the waveguide thickness-averaged nonlinear addition to the refractive index. Photorefraction in waveguides on the Z-cut of the $3m$ symmetry crystals with the dominating photovoltaic mechanism is determined by the redistribution of charges along the polar axis and the linear electrooptical effect, and can be described by an integral expression, which takes into account the inhomogeneity of the light-field distribution and of photorefractive properties of the medium over the coordinate z. Ti : Fe : $LiNbO_3$ waveguide structures, in which the dark conductivity substantially exceeds the photoconductivity, exhibit optical nonlinearity of the Kerr type. Dark spatial solitons in such planar waveguides can be obtained at different selectively excited waveguide modes in the case of the appropriate inhomogeneous distribution of the amplitude over the transverse coordinate orthogonal to the polar axis z.

The numerical analysis performed in the paper has shown that single-mode beams modelling dark spatial solitons can propagate in real Z-oriented planar Ti : Fe : $LiNbO_3$ waveguides when the input beam power is ~ 1 mW. Note that dark spatial solitons were experimentally observed in the stationary regime in Ti : Fe : $LiNbO_3$ waveguides fabricated on the Y-cut substrates at comparable light powers [6].

Acknowledgements. This work was supported by the INTAS (Grant INTAS-01-0481). M.V. Borodin thanks the Yukos oil company for financial support.

References

1. Stegeman G.I., Segev M. *Science*, **86**, 1518 (1999).
2. Segev M., Crosignani B., Yariv A., Fisher B. *Phys. Rev. Lett.*, **68**, 923 (1992).
3. Iturbe-Castillo M.D., Marquez Aguilar P.A., Sanchez-Mondragon J.J., Stepanov S., Vysloukh V. *Appl. Phys. Lett.*, **64**, 408 (1994).
4. Valley G.C., Segev M., Crosignani B., Yariv A., Fejer M.M., Bashaw M.C. *Phys. Rev. A*, **50**, R4457 (1994).
5. Taya M., Bashaw M.C., Fejer M.M., Segev M., Valley G.C. *Opt. Lett.*, **21**, 943 (1996).
6. Shandarov V., Kip D., Wesner M., Hukriede J. *J. Opt. A: Pure Appl. Opt.*, **2**, 500 (2000).
7. Chauvet M., Chauvin S., Mailotte H. *Opt. Lett.*, **26**, 1344 (2001).
8. Kip D., Wesner M., Shandarov V., Moretti P. *Opt. Lett.*, **23**, 921 (1998).
9. Hukriede J., Nee I., Kip D., Kratzig E. *Opt. Lett.*, **23**, 1405 (1998).
10. Popov V.L., Shandarov V.M. *Zh. Tekh. Fiz.*, **61**, 88 (1991).
11. Kip D. *Appl. Phys. B*, **67**, 131 (1998).
12. Kip D., Hukriede J., Kratzig E. *Phys. Stat. Sol.*, **168**, R3 (1998).
13. Hukriede J., Kip D., Kratzig E. *J. Opt. A: Pure Appl. Opt.*, **2**, 481 (2000).
14. Tamir T. (Ed.) *Volnovodnaya optoelektronika* (Waveguide Optoelectronics) (Moscow: Mir, 1991).
15. Goncharenko A.M., Red'ko V.P. *Vvedenie v integral'nuyu optiku* (Introduction to Integrated Optics) (Minsk: Nauka i Tekhnika, 1975).
16. Sturman B.I., Fridkin V.M. *Fotogal'vanicheskii effekt v sredakh bez tsentra inversii i rodstvennye yavleniya* (Photogalvanic Effect in Media without the Symmetry Centre and Related Phenomena) (Moscow: Nauka, 1992).
17. Landau L.D., Lifshits E.M. *Kvantovaya mekhanika* (Quantum Mechanics) (Moscow: Nauka, 1988).
18. Larionov Yu., Shandarov S., Shandarov V. *Nonlinear Guided Waves and Their Applications. OSA Tech. Digest* (Washington: OSA, 1997) pp 65–167.
19. Nisius J.P., Kratzig E. *Sol. St. Commun.*, **53**, 743 (1985).
20. Barkan I.B., Vorob'ev A.V., Marennikov S.I. *Kvantovaya Elektron.*, **6**, 833 (1979) [*Sov. J. Quantum Electron.*, **9**, 492 (1979)].
21. Shaskol'skaya M.P. (Ed.) *Akusticheskie kristally. Spravochnik* (Handbook of Acoustic Crystals) (Moscow: Nauka, 1982).